PIV APPLICATION TO MACH 3.75 OVEREXPANDED JET

by

A. Jerónimo; M. L. Riethmuller; O. Chazot

Von Karman Institute for Fluid Dynamics

Abstract

The velocity field of a Mach 3.75 overexpanded jet was investigated using Particle Image Velocimetry. The jet was produced by a conical nozzle discharging in quiescent ambient air and connected to a settling chamber whose pressure was set to 25 bar. 170 instantaneous image pairs were cross-correlated using final window size of 16x24 pixels which corresponded to a spatial resolution of 0.544 mm and 0.816 mm in the streamwise and transverse directions, respectively. The mean flow quantities such as velocity, velocity divergence, vorticity, as well as the turbulence intensities were computed and analysed providing information on jet structure. The problems related to the PIV application to supersonic flows were addressed and discussed, such as, response of seeding particles to flow accelerations, image processing uncertainty and shock wave oscillation. The results were compared with theory and showed good agreement except in the location of the Mach disk where the effect of particle inertia was evident. The comparison with schlieren images showed that all the flow structures were identified as well as their geometry and location were in very good agreement with the schlieren image.

1 Introduction

The flow field produced by supersonic nozzles has received considerable attention for a long time. This interest is motivated by the development of air and space propulsion systems, such as solid rocket motor, with high-performance nozzle design, providing improved thrust and enhanced jet plume mixing (Hamed and Vogiatzis, 1998; Yuceil et al, 2000). Although the nominal design conditions of these systems, correspond to ideally expanded nozzles, when at sea-level the flow is often overexpanded and separation inside the nozzle can occur causing unexpected nozzle side loads (Romine, 1998). Despite the practical interest of this type of flows, there is still a lack of knowledge on the mean and turbulent flow structure. The use of physical probes in small-scale supersonic flow experiments has demonstrated to be very intrusive, therefore the use of non-intrusive optical methods reveals to be a more adequate experimental approach to these flows.

Particle Image Velocimetry is a non-intrusive optical technique, which has demonstrated to be efficient in providing detailed mean and turbulent flow information in a plane. The principles of this technique have been extensively described in the literature (Adrian, 1991; Willert and Gharib, 1991; Riethmuller, 1996). At the present time, its applicability to subsonic flows is well assessed and documented, however, PIV applications to supersonic flows still constitute a challenge. During the last ten years, several investigations have been performed concerning the extension of PIV applications to high-speed and supersonic flows highlighting specific issues (Molezzi and Dutton, 1993; Krothapalli et all, 1994; Raffel et al, 1996; Lawson et al, 1999). The main problem concerns the seeding technique, since the large flow rates in supersonic flow involve significant seeding quantities in a flow field that is subjected to large gradients. Therefore uniform seeding concentrations are very difficult to obtain and special care has to be taken in selecting the adequate seeding technique (Meyers, 1991). Another problem that has been addressed in literature is the size of seeding particles required to follow the flow during the acceleration process. The particles should be as small as possible, but still scattering sufficient amount of light to be detected by the camera, therefore a compromise has to be made in the particle size and powerful lasers are required to illuminate the flow field (Raffel et al, 1997).

The present work concerns PIV application to a Mach 3.75 overexpanded jet. Special care was taken in the choice of the seeding particles and in the seeding generation device.

2 Experimental Approach

2.1 Supersonic Jet Facility

The jet flow is generated by a conical nozzle having 113 mm length with throat and exit diameters of D_t=5.85 mm and D_e=17.3 mm, respectively, which corresponds to fully expanded Mach number Ma=3.78. The jet exhausts in quiescent air at ambient conditions (P_{amb} = 1 bar and T_{amb}= 290 K). The nozzle is connected to a settling chamber whose pressure can be varied by means of an upstream valve, although the results presented in this work refer to a fixed total pressure of 25 bar. The jet uses dried air from a 40 bar supply tank and it can be run continuously for several hours before the tank has to be recharged. The information on the total pressure in the settling chamber is provided by a Bourdon type manometer. Upstream of the settling chamber, air mixes with oil seeding particles produced by a Laskin's nozzle seeding generator. This device was already existing at the Von Karman Institute Laboratory, although several modifications were introduced by the authors, namely a new impactor was designed, in order to have sub-micron particles at the measurement section (Jeronimo, 2001).

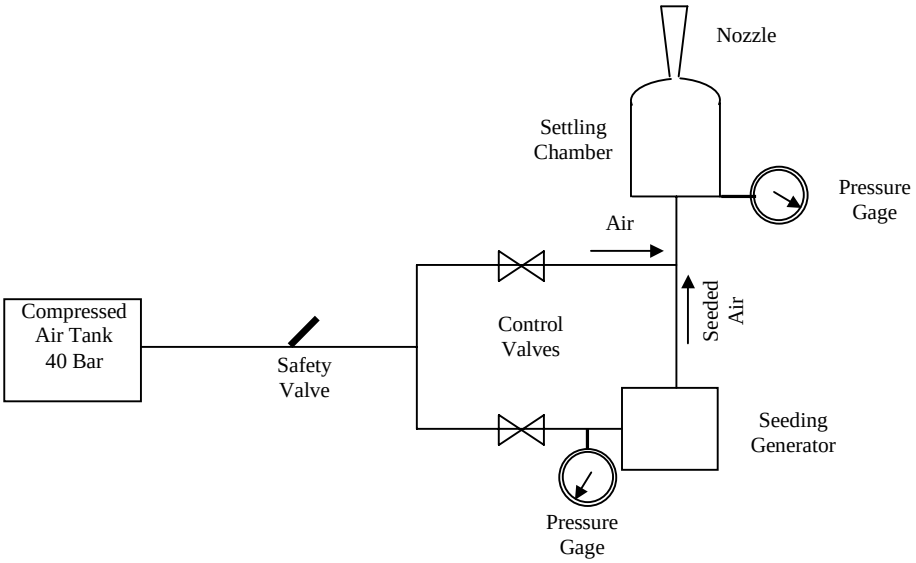

Figure 1 – Supersonic Jet Facility

2.2 PIV System Set-Up

In this experiment a pulsed Nd:Yag laser of 200mJ/pulse energy was used. The wavelength of the laser beam is 532 nm. The laser sheet was formed by means of a cylindrical and spherical lens and was 0.5 mm thick at the measurement section.

The synchronization of both Camera and Laser was achieved by the combination of a Signal Generator and a Delay Generator. The Signal Generator produced an 8.2 Hz triggered signal sent to both Camera and Delay Generator. The later was used to trigger the Laser with a delay of 1.23 microsecond with respect to the original signal sent to the Camera. This procedure was necessary to achieve a pulse separation of 0.5 μs. The Laser pulse separation was also imposed by the Delay Generator.

The PIV images were acquired with a 12 bits PCO Digital Camera, which has a nominal spatial resolution of 1280x1024 pixels and sampling frequency of 4.12 Hz. The imaged area was approximately 4x2 cm, corresponding to 1280x544 pixel. This allowed a higher sampling frequency of 8.2 Hz. The Nikon objective was working with a 50 mm lens mounted on the Camera using an extension ring. The Camera diaphragm was open to an f number of 5.6.

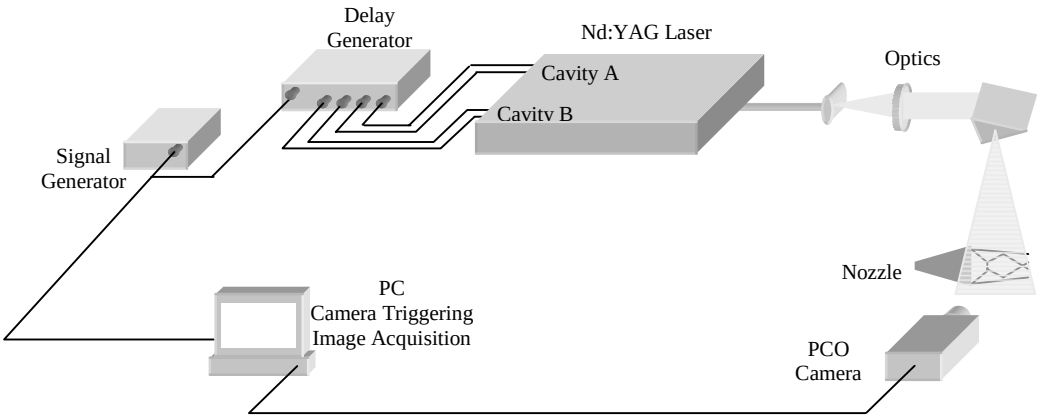

Figure 2 – PIV System Set-Up

2.3 Image Processing

Because of the limited time available for the experiments, only 170 image pairs were recorded. These were cross-correlated with WIDIM software developed at the VKI. This software uses iterative windows displacement and windows distortion (Scarano and Riethmuller, 1999). The final size of the interrogation windows was 16 pixels in the horizontal direction and 24 pixels in the vertical direction, since the largest velocity gradients, corresponding to the flow across shock waves, are in the horizontal direction. With these conditions we obtain a spatial resolution of 0.544 mm and 0.816 mm in the horizontal and vertical directions respectively. 75 % of final window overlap was used yielding vector spacing of 0.128 mm and 0.204 mm in the horizontal and vertical directions, respectively. The global Signal-to-Noise Ratio was approximately 3.

3 PIV Results

Mean flow quantities were computed from an ensemble of 170 instantaneous flow fields, enabling calculation of different mean flow quantities, such as, velocity, vorticity, velocity gradients and velocity divergence. Statistical analysis of the flow provided streamwise and transverse velocity rms. These quantities were used to assess streamwise and transverse turbulence intensities. Although the number of samples used to perform the statistical analysis is not sufficient to accurately describe turbulence intensities, the obtained curves provide insight on the turbulent nature of the flow. The axial and transverse coordinates were dimensionalized by the nozzle outlet diameter and the rms velocity fluctuation is normalized with jet outlet freestream velocity.

3.1 Validation of the Results

Before proceeding with the analysis of the flow field based on the PIV results, it is convenient to assess the accuracy of the technique for the experimental conditions. Since the supersonic flow field is characterized by strong accelerations of the flow across shocks and expansions, problems of tracer fidelity across shockwave as well as the error from image processing at shock location where the gradients are very large, should be discussed.

3.1.1 Image Processing Uncertainty

(Scarano and Riethmuller, 2000) discusses the error committed by WIDIM image processing on the measured displacement of particles. The error is basically a function of the final window size, particle displacement and the

displacement gradients within one window size. For the present conditions, one retrieve that the maximum error is observed at the normal shock location (figure 3), where the maximum displacement gradient measured is 0.23 pixels/pixel and the displacement error is 0.3 pixels. This error is relatively large and corresponds to a velocity uncertainty of ± 22 m/s at the mach disk location providing a maximum error of ± 11.6 % of the measured velocity at this location. For the freestream flow the error is estimated to be less than ± 4 m/s or 0.5% of the measured velocity.

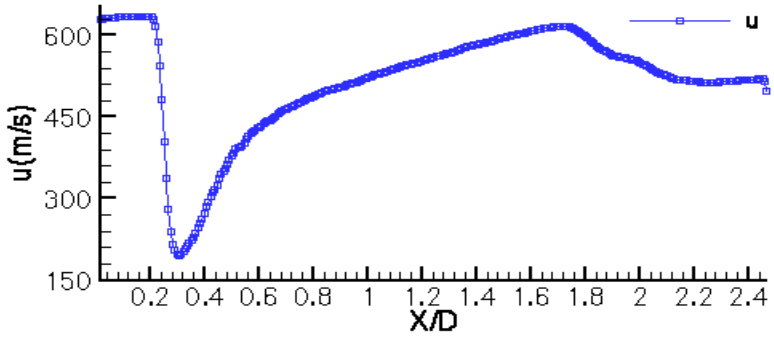

Figure 3 – Mean Streamwise Velocity on Jet Centreline

3.1.2 Particle Dynamics and Frequency Response of Seeding Particles.

One of the main problems of PIV application to high speed flows lays on proper tracer particles selection. Due to the high velocity gradients the particles should be as small as possible. However, for sake of particle imaging it is required that particles are large enough to scatter sufficient amount of light, meaning that a compromise should be made on particle size.
For PIV applications the particle's response is conveniently described by the relaxation distance or the relaxation time required, for the particle velocity lag (Up-Uf), after a shock wave to be reduced by a factor of 1/e=0.368 (Melling, 1997). In the present case, the incident oblique shock represented in figure 4 is used to perform such analysis. The PIV data corresponding to the velocity component normal to the shock was extracted along the black line drawn in figure 4. The variation of particle normal velocity with normal distance can be directly extracted from PIV results and be used to infer variation of particle normal velocity with time. This result is shown in figure 5.

The simplified equation of particle motion in gas flow can be expressed by (Melling, 1997):

$$\frac{d\vec{U}_P}{dt} = -C(\vec{U}_P - \vec{U}_f);$$

Where C is a characteristic frequency of particle motion.

The solution of this equation is of the form

$$\left|\frac{\vec{U}_F - \vec{U}_P}{\vec{U}_F - \vec{U}_{Pi}}\right| = e^{-Ct},$$

and the relaxation time is simply 1/C.

Therefore, the exponential fit to the experimental data in figure 5 provided particle relaxation time of approximately τ=1.5μs, corresponding to a particle frequency response of 667 kHz.

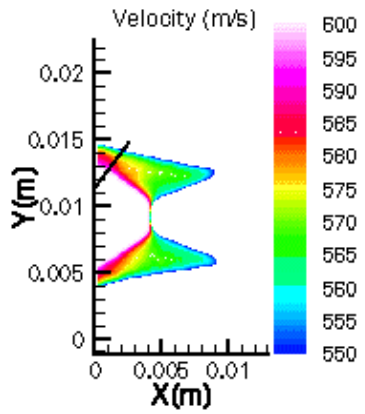

Figure 4 – Zoomed Velocity Contour Plot on Oblique Shock

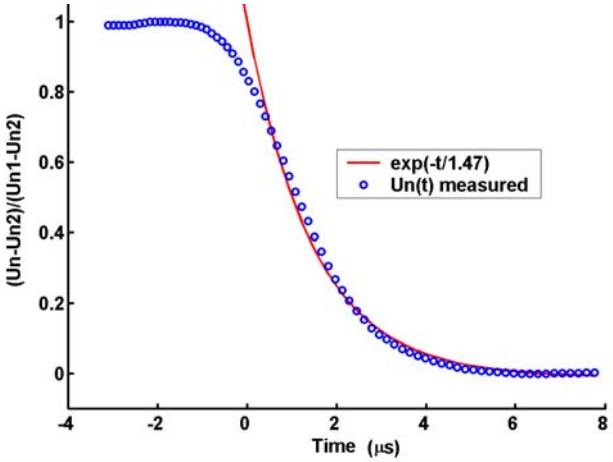

Figure 5 – Particle Relaxation Time across Oblique Shock

3.1.3 Schlieren Image Analysis and Comparison with PIV Results

Schlieren image technique allows detection of shock waves, expansion fans and slip lines, which are features present in an overexpanded jet. This technique provides more than qualitative information, since shock wave angles are related to Mach number changes, thus velocity changes, across shock waves. The purpose of this section is to examine the structure of the overexpanded jet and estimate mean flow quantities to be compared with the PIV results.

Figure 6 is a schlieren image of the overexpanded jet considered in the present work. It shows a characteristic shock cell pattern that has been extensively described in the literature (Love et al, 1959; Frey, 1998). The incident shock waves are obviously forming at the nozzle wall, rather than at the nozzle lip, which is a clear indication that separation of the boundary layer is occurring inside of the nozzle. Reference (Romine, 1998) provides modelling of flow separation in overexpanded nozzles allowing calculation of the free stream Mach number at separation and at triple point. This last result is interesting for comparison with the PIV measured velocity at the jet centreline and before the Mach disk. Therefore, for an estimated triple point Mach number of Ma=3.75 and considering isentropic flow expansion from stagnation conditions, the estimated freestream velocity before the Mach disk is 655 m/s, which differs from the measured velocity of 640 m/s within +2.3%.

The assumption of adiabatic flow across the Mach disk normal shock provides estimation of the velocity after this shock to be 147 m/s. The comparison of this value with the PIV results at the same location and shown in figure 3, presents a difference of -22.5 % of the measured velocity. This difference is larger than the uncertainty calculated at this location, meaning that the seeding particles have not completely relaxed at this location. This is most probably due to the combination of the strong deceleration imposed by the normal shock and the large acceleration of the flow after the Mach disk.

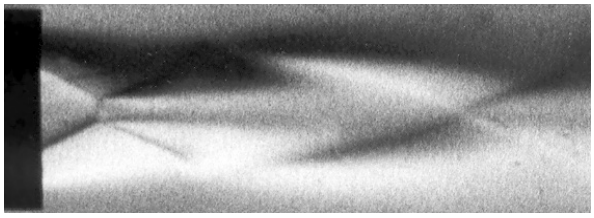

Figure 6 – Schlieren Image of Overexpanded Jet

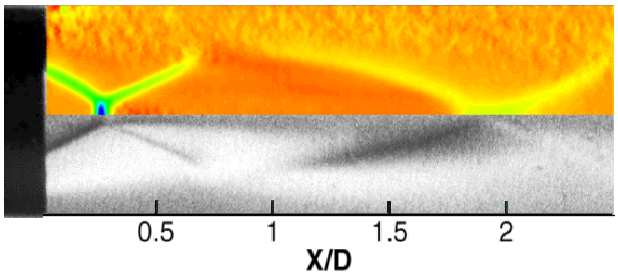

Figure 7 – PIV Comparison with Schlieren Image

Figure 7 shows the mean velocity divergence ($\frac{\partial u}{\partial x}+\frac{\partial v}{\partial y}$) contour plot, calculated from the PIV velocity field and superposed to the jet schlieren image of figure 6. In the contour plot, one can easily identify the incident oblique shock, the strong Mach disk compression and the reflected oblique shock. After the Mach disk the flow is expanding until the next incident oblique shock of the second shock cell. All these features are in good agreement with the shock pattern obtained from schlieren visualization.

3.2 Instantaneous Velocity Field

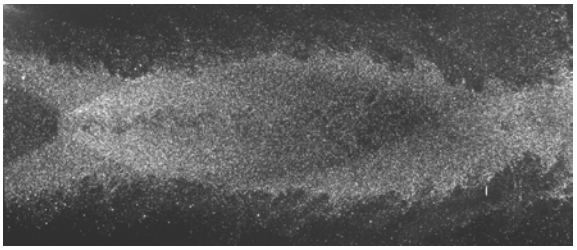

Figure 8 – Typical Instantaneous PIV Image

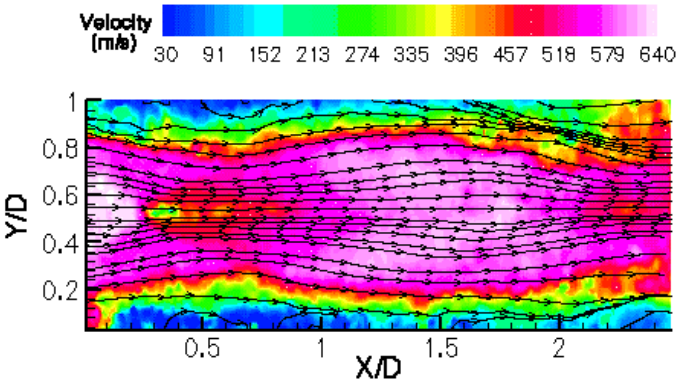

Figure 9 – Instantaneous Velocity Contour Plot and Streamlines

Figure 8 is a typical PIV instantaneous image obtained for the flow exiting from the overexpanded nozzle. The seeding concentration was kept high in order to increase the spatial resolution and the global Signal-to-Noise Ratio of the measurements. The ideal condition of uniform seeding concentration in the measurement section cannot be respected for flow with strong density variations, as the present case.
Since only the flow exiting from the nozzle was seeded, one can only obtain high Signal-to-Noise ratio in the core of the jet, although the results obtained for the complete field of view show that even the shear layers could be resolved.

Figure 9 shows the instantaneous velocity contour plot and velocity stream traces. The flow decelerations across the oblique and normal shock are well visible, as well as the change of the velocity direction across the oblique shocks. Outside of the jet core the densely spaced contour levels show the shear layers developing at the jet boundary. The stream traces at this region show entrainment of the outside flow in the shear layers, shear layer growth and its penetration into the jet core.

3.3 Analysis of the Mean and Turbulent Flow Fields

Figure 10 shows the mean velocity field contour plot and flow streamlines. The flow exiting from the nozzle is at a pressure substantially lower than the surrounding atmospheric pressure. Thus the supersonic flow as to adapt to ambient pressure. For the flow at the nozzle centreline, the pressure recovery is done in one step through a Mach disk. The velocity after this normal shock is subsonic. For the surrounding flow, the compression to ambient pressure is done in two steps through two pairs of oblique shock waves. The streamlines are curved as they pass the first incident oblique shocks to be again aligned with the axis after the second pair of oblique shocks. The velocity after these oblique shocks is still supersonic. Thus the flow after the Mach disk presents a velocity discontinuity at the intersection points of the oblique shocks with the Mach disk, the so-called triple points. From schlieren visualization of figure 6, one can see two slip lines emanating from the triple points. These lines can also be observed in the vorticity contour plot of figure 11, as two regions of high vorticity level developing downstream of the Mach disk. Indeed, at this region also the streamwise turbulence intensity is increased, as shown on figure 12 and turbulent mixing between the subsonic and supersonic

flows, takes place causing the growth of two shear layers merging at the jet centreline and developing as a Mach disk wake.

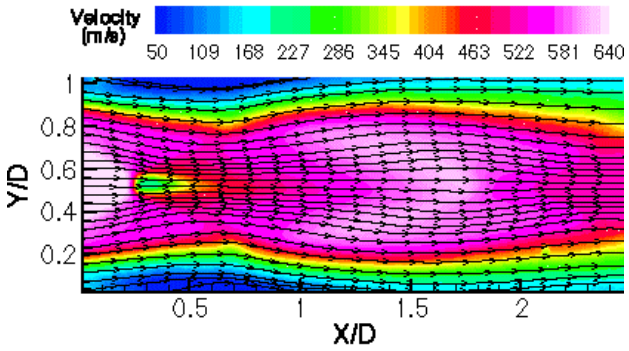

Figure 10 – Mean Velocity Contour Plot and Streamlines

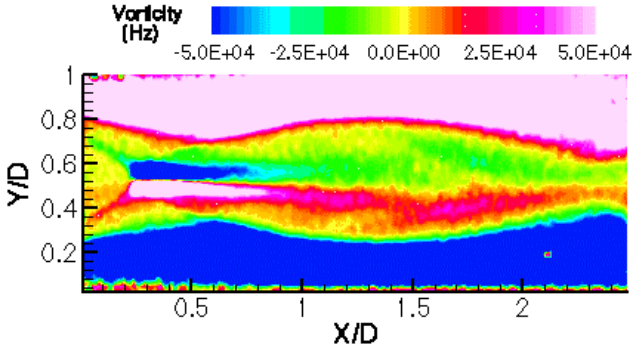

Figure 11 – Mean Vorticity Contour Plot

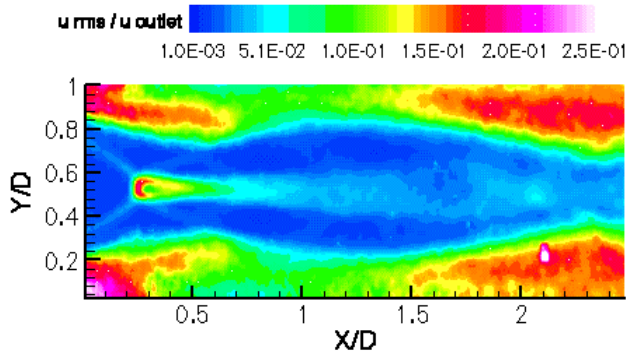

Figure 12 – Streamwise Turbulence Intensity Contour Plot

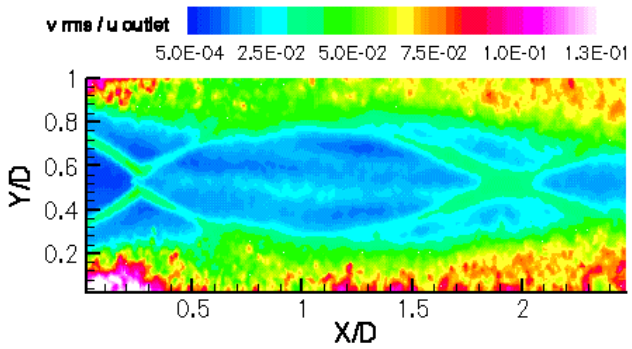

Figure 13 – Transverse Turbulence Intensity Contour Plot

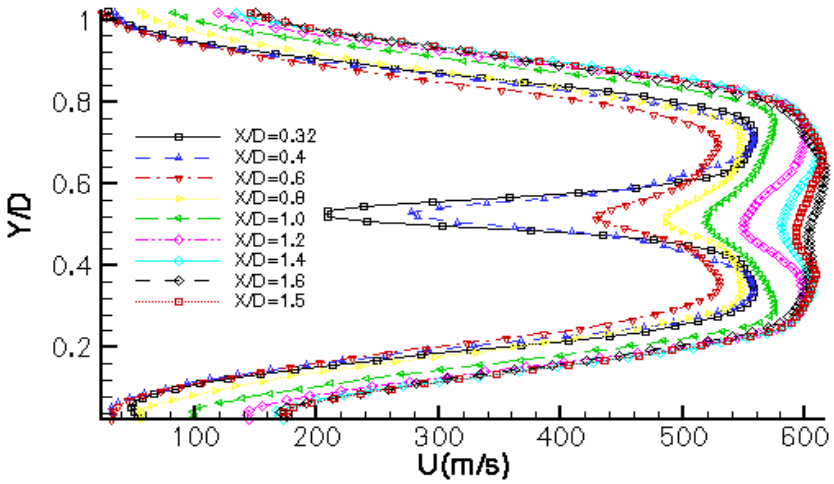

Figure 14 – Transverse Profiles of Mean Streamwise Velocity

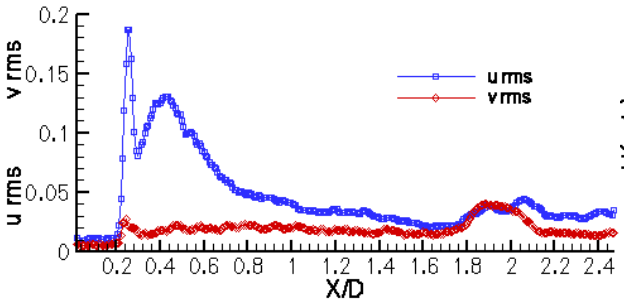

Figure 15 – Streamwise and Transverse Turbulence Intensities on Jet Centreline

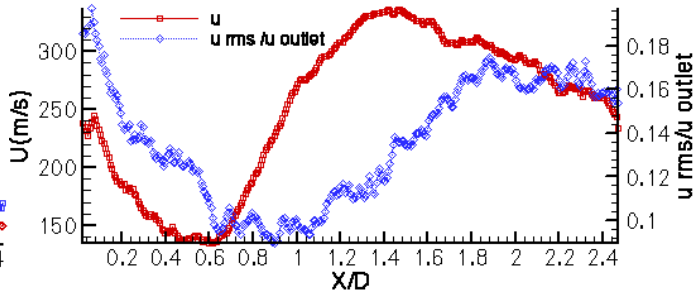

Figure 16 – Mean Velocity and Streamwise Turbulence Intensity on Y/D=0.92

From the analysis of figure 3, it is observed a strong increase on the streamwise velocity until X/D≡0.6, after this point the increase in velocity is weaker. Figure 14 provides information on the streamwise velocity profiles developing after the Mach disk. For the profiles corresponding to X/D≤0.6 it is observed that the increase in streamwise velocity on jet centreline corresponds to a decrease in the streamwise velocity outside of the Mach disk region. If now, we consider the velocity profiles corresponding to X/D≥0.7 it is verified that not only in the jet centreline, streamwise velocity is being increased but, also in all the values of the transverse coordinate (Y/D). The streamwise turbulence intensity profile on figure 15 reveals a very intense peak at the Mach disk location, with a maximum value of 0.19 that immediately drops to 0.08. This behaviour of the turbulence intensity across shock waves has been already reported in the literature (Yuceil, 2000) and will be studied in further detail in section 3.4. After this streamwise turbulence intensity peak, turbulence increases again and remains high until X/D≈0.6. As conclusion of the previous statements one might say that the increase in streamwise velocity on jet centreline and after the Mach disk is due to two different phenomena. The first, corresponding to the steep increase in the velocity and taking place until X/D≈0.6 is dominated by turbulent mixing and shear layer growth, to which corresponds high levels of turbulence and vorticity. The mild increase in streamwise velocity at jet centreline for X/D>0.6 is most probably due to expansion of the flow. Indeed, when the second oblique shock reaches the jet boundary an expansion fan is formed and the flow undergoes expansion. From the velocity divergence plot and from schlieren observation in figure 7, the location of the expansion on jet boundary is approximately X/D≈0.6.

The jet boundary shear layers reveal high levels of vorticity and turbulence intensity. In figure 12 it is observed a decrease in streamwise turbulence intensity in the jet boundary shear layers at the location of the expansion fan. Figure 16 confirms this observation at Y/D=0.92 and it is verified that the streamwise turbulence intensity drops from approximately 0.2 to 0.08.

The previous observations reveals that the flow field in the plume of an overexpanded jet is highly non-uniform and turbulence is clearly anisotropic.

3.4 Velocity RMS and Shock Wave Oscillation

The analysis of the flow fluctuations revealed a large peak in streamwise velocity fluctuation at the Mach disk location. A detailed investigation of the causes of such high peak was performed taking into account the individual analysis of the 170 instantaneous velocity fields.

Figure 17 shows instantaneous velocity profiles along the jet centreline at the region of the Mach disk normal shock. The results clearly show streamwise shock oscillation within an amplitude of approximately 1 mm. This unsteady behaviour is probably due to interaction between the separated turbulent boundary layer and the oblique shocks forming at the nozzle wall.

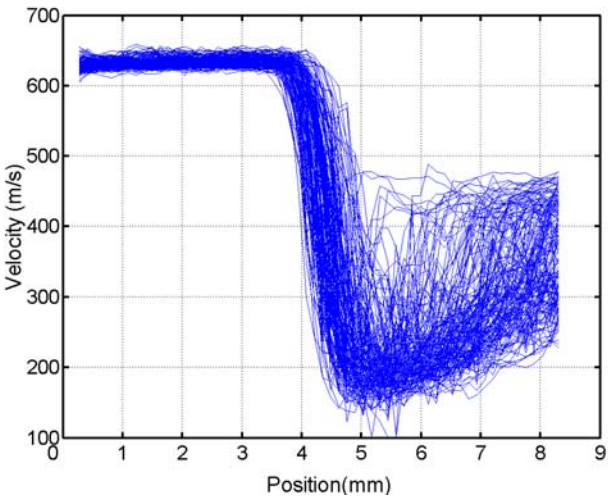

Figure 17 – 170 Instantaneous Velocity Profiles Across the Mach Disk Centreline

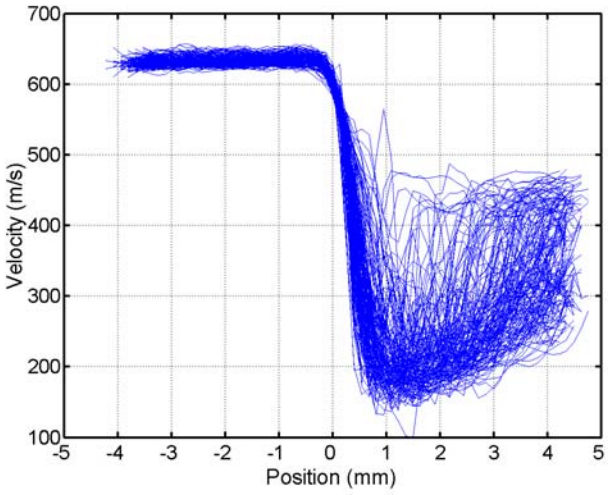

Figure 18 - 170 Instantaneous Velocity Profiles Across the Mach Disk Centreline with Shock Alignment

Because one would like to access the effect of this unsteady behaviour on the mean and turbulent velocity fields, a different method for the calculation of the mean velocity field was considered. The method relies on detection of normal shock relative position for each instantaneous velocity field. This is achieved by fitting a 10^{th} order polynomial to the instantaneous velocity across the shock, which considerably reduced the noise level. The reference point for shock alignment was inferred from the instantaneous velocity fit, as the axial position corresponding to a velocity of 600 m/s. The value of each reference point in each velocity field was subtracted to the axial coordinate and the alignment of shock position is made at X=0, as shown in figure 18.

The comparison of the results provided by the previous method, with the results obtained in section 3.3 are shown in figures 19, 20, 21 and 22.

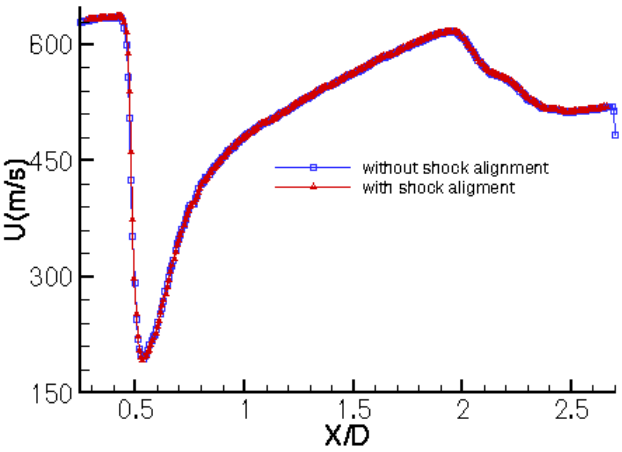

Figure 19 – Comparison of Mean Streamwise Velocity at Jet Centreline

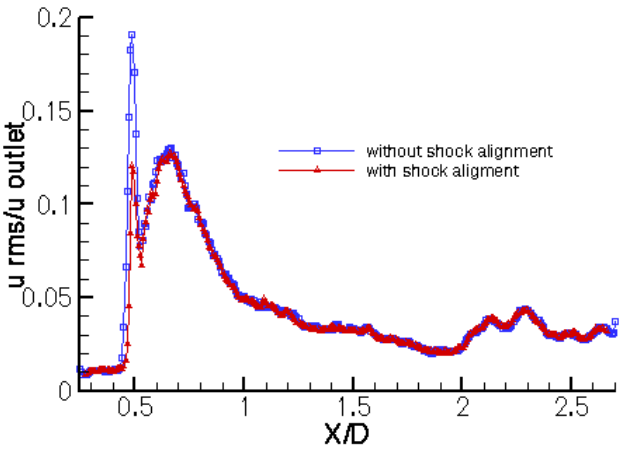

Figure 20 – Comparison of Streamwise Turbulence Intensity at Jet Centreline

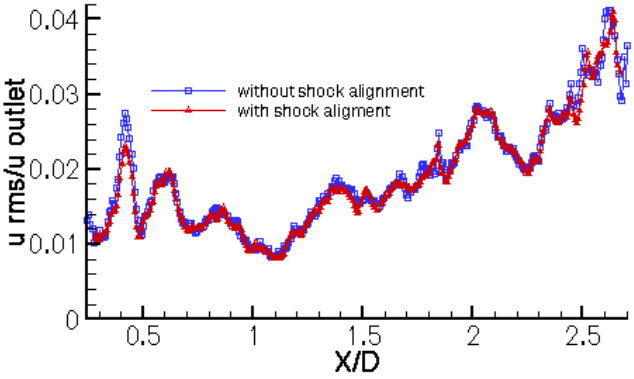

Figure 21 – Comparison of Mean Streamwise Velocity at Jet Centreline

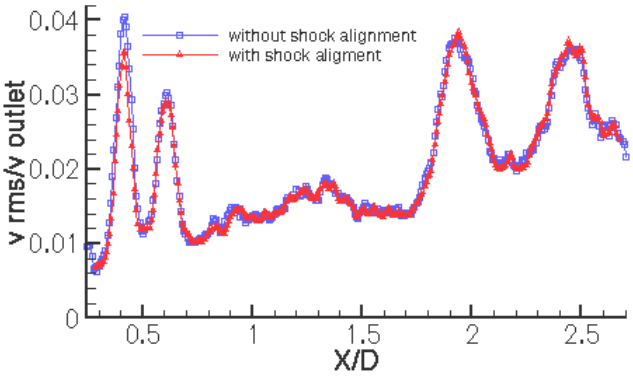

Figure 22 – Comparison of Streamwise Turbulence Intensity at Jet Centreline

The comparison of the results provided by the previous method, with the results obtained in section 3.3 are shown in figures 19, 20, 21 and 22. As it is expected, the differences between the results in the mean velocity field are negligible. However the velocity fluctuations at shock location are significantly decreased when shock alignment is considered. Indeed, the streamwise velocity fluctuation at Mach disk location shown in figure 20 is decreased by 31.5%, while the transverse and streamwise velocity fluctuations at the oblique shock are decreased by 12% and 14% respectively, as shown in figures 22 and 21, respectively. In the remaining flow field there were no significant differences in the turbulence intensities. Therefore, one should take into consideration that large turbulence intensities in the vicinity of shock waves should not be seen as turbulence, but rather as the consequence of shock wave oscillation. Also particle relaxation length or time, are often overestimated when considered across oscillating shocks.

4 Conclusions

The supersonic flow field of a Mach 3.75 overexpanded jet was experimentally investigated by means of Particle Image Velocimetry. Typical problems of PIV applications to supersonic flows with large velocity gradients were addressed and discussed. The frequency response of the seeding particles was estimated on the basis of particle relaxation time across the incident oblique shock, providing a value of 667 kHz. Despite the relatively large value encountered for the frequency response of particles, the velocity lag after the Mach disk was estimated to be approximately 22.5% of the local flow velocity, although 91% of the velocity step can be resolved. Uncertainty analysis of image processing technique provided a minimum error of ±0.5% at the freestream jet exit velocity, while the maximum error of ±11.6% occurred at the Mach disk location. The latter was due to the large velocity gradients. The 170 instantaneous velocity profiles at jet centreline were analysed showing that the normal shock Mach disk was oscillating with amplitude of 1 mm in the streamwise direction. A new average and turbulent field were derived considering alignment of the 170 instantaneous flow fields, in order to have the Mach disk position in each field at the same relative location. This procedure revealed to be efficient in reducing the rms velocity fluctuation at the Mach disk by a factor of 31.5%, as well as, at the oblique incident shock waves. However, the differences between the two mean velocity fields, derived by the normal average procedure and the one considering shock alignment, were not significant. One might conclude that when analysing the turbulent flow field obtained in the vicinity of shock waves, the velocity fluctuations may not correspond to turbulence, but rather to an unsteady oscillation of the shock waves. Also velocity frequency response of particles is often underestimated when derived from particle response across oscillating shocks.

The analysis of the mean and turbulent velocity field showed that all the flow structures characteristic of overexpanded supersonic jets were resolved, such as incident and reflected oblique shocks, expansion fans, Mach disk and slip lines. The analysis of the streamwise velocity profiles at different values of X/D coordinate after the Mach disk, revealed intense momentum transfer in the transverse direction, corresponding to the shear layers developing at the slip lines. The steep acceleration of the flow at the jet centreline and after the Mach disk, is dominated in an initial part (until values of X/D = 0.6 - 0.7) by turbulent mixing and shear layer growth, after this point, the increase in velocity is milder, corresponding to a global flow acceleration caused by expansion. This argumentation is supported by the observations in the mean vorticity and turbulent fields. The flow field is non-uniform and turbulence is clearly anisotropic.

Comparison of the mean velocity divergence field with schlieren images, showed very good agreement in terms of identification of flow features, as well as their geometry and location. PIV is shown to be an adequate technique in the assessment of the mean and turbulent fields of an overexpanded jet with large velocity gradients, except in the region of the Mach disk because of particle velocity lag and image processing uncertainty.

References

Adrian, R. J. 1991 Particle imaging techniques for experimental fluid mechanics, *Ann. Rev. Fluid Mech.* Vol. 23.

Frey, M. 1998 Shock patterns in the plume of overexpanded rocket nozzles. *Proc. 3rd European Symp. Aerothermodynamics for Space Vehicles*, ESTEC, Noordwijk, The Netherlands.

Hamed, A. & Vogiatzis, C. 1998 Overexpanded two-dimensional convergent-divergent nozzle performance, effects of three-dimensional flow interactions. *J. Prop. Power*, vol.14, no 2.

Jerónimo, A. 2001 *Application of PIV to a supersonic jet.* VKI PR 2001-28.

Krothapalli, A., Whishart, L. M. & Lourenço, L. M. 1994 Nearfield structure of a supersonic jet: On line PIV study. *Proc. 7th International Symp. Appl. Laser Tech. Fluid Mech.,* Lisbon, Portugal.

Lawson, N. J., Page, G. J., Halliwell, N. A. & Coupland, J. M. 1999 Application of particle image velocimetry to a small-scale de Laval nozzle. *AIAA journal*, vol.37, no 7.

Love, E. S., Grigsby, C. E., Lee, L. P. & Woodling, M. J. 1959 Experimental and theoretical studies of axisymmetric free jets. *NASA,* TR R-6.

Melling, A. 1997 Tracer particles and seeding for particle image velocimetry. Meas. Sci. Technology, vol. 8, pp. 1406-1416.

Meyers, J. F. 1991 Generation of particles and seeding. *VKI LS 1991-05*

Molezzi, M. J. & Dutton, J. C. 1993 Application of particle image velocimetry in high speed separated flows. *AIAA journal*, vol. 31, no.3.

Raffel, M., Willert, C. E. & Kompenhans, J. 1997 *Particle image velocimetry: A practical guide*. Springer

Raffel, M., Höfer, H., Kost, F., Willert, C. & Kompenhans, J., 1996 Experimental aspects of PIV measurements of transonic flow fields at the trailing edge model of a turbine blade. *Proc. 8th International Symp. Appl. Laser Tech. Fluid Mech.*, Lisbon, Portugal.

Riethmuller, M. L. 1996 Particle image velocimetry. *VKI LS* 1996-03.

Romine, G. L. 1998 Nozzle flow separation. *AIAA journal*, vol. 36, no 9.

Scarano, F. & Riethmuller, M. L. 1999 Iterative multigrid approach in PIV image processing with discrete window offset. *Experiments in Fluids*, vol. 26, pp 513-523.

Scarano, F. & Riethmuller, M.L. 2000 Advances in iterative multigrid PIV image processing. Experiments in Fluids, vol. 29.

Willert, C. E. & Garib, M. 1991 Digital particle image velocimetry. *Experiments in Fluids*, no 10, 181-193.

Yüceil, K.B., Ötügen, M.G. & Arik, E. 2000 Underexpanded sonic jets: A PIV study. *Proc. 10th International Symp. Appl. Laser Tech. Fluid Mech*, Lisbon, Portugal, 2000.